

The Dynamical and Microphysical Structure of an Occluded Frontal System and its Modification by Orography¹

PETER V. HOBBS, ROBERT A. HOuze, JR., AND THOMAS J. MATEJKA

Department of Atmospheric Sciences, University of Washington, Seattle 98195

(Manuscript received 4 February 1975, in revised form 5 May 1975)

ABSTRACT

An occluded front moving over Washington State was investigated with serial rawinsonde ascents, aircraft penetrations, raingage measurements and conventional observations.

The rawinsonde data showed that the frontal system contained alternate mesoscale tongues of air with low and high values of wet-bulb potential temperature (θ_w). These tongues included a pre-frontal surge of low- θ_w air aloft, centered at about the 700 mb level, a low-level high- θ_w tongue along the front, and two post-frontal high- θ_w tongues. The low- and high- θ_w tongues were of the order of 50–100 km in width.

The frontal precipitation was confined to a mesoscale band, 80 km in width, along the front. The cloud associated with this band was characterized by a vertical circulation similar to, but much less vigorous than, an organized convective system. Cloud microphysical data indicated that a narrow cumulus-scale updraft zone was located near the leading edge of the frontal cloud. The concentrations of ice particles in the frontal cloud were probably on the order of $50 \ell^{-1}$ but could have been as high as $500 \ell^{-1}$. These values exceed the optimum for the efficient release of precipitation by the Bergeron-Findeisen process. However, cloud particles collected in flight revealed that both riming and aggregation played important roles in particle growth within the frontal cloud.

As the frontal system passed over the Cascade Mountains, the amount of cloud and precipitation ahead of the front decreased while that behind the front increased. The decrease in cloudiness ahead of the front is attributed to the low-level moisture source being cut off by the mountains. The increase in clouds behind the front was apparently due to orographic lifting of the cold air.

This study confirms that mesoscale processes play an important role in the production of frontal precipitation. It also indicates that the microphysical aspects of precipitation growth are more complex than classical models would suggest.

1. Introduction

Much evidence has been accumulated in the past decade concerning the complexity of precipitation processes in extratropical cyclones. One of the most important realizations has been that mesoscale² processes play a crucial role in these systems. Studies by Kreitzberg (1964), Elliott and Hovind (1965), and Kreitzberg and Brown (1970) have shown that the idealized frontal zones of the classical synoptic models introduced by Bjerknes (1919) are, in fact, often composed of several intensely baroclinic mesoscale subzones embedded within a relatively large transition zone.

Elliott and Hovind (1964) found that the rainfall from frontal systems passing over California was typically concentrated in a series of bands, each from 35 to 60 km in width and of the order of 100 km in length. These bands were embedded in a general synoptic precipitation pattern and contained within them cumu-

lus-scale precipitation cells. Similar hierarchical structures in the precipitation patterns of fronts and cyclones have been described by Browning and Harrold (1969), Austin and Houze (1972), and Harrold (1973).

The key microphysical aspect of precipitation growth in mid-latitude clouds has long been thought to be the growth of ice particles by diffusion of vapor from supercooled drops, as postulated by Bergeron (1935). However, Houghton (1968) has shown that this "ice-crystal process" is likely to be effective only under very idealized conditions, namely in stratiform clouds in which the ice particle concentrations do not exceed typically measured concentrations of ice nuclei (about $1 \ell^{-1}$ at -20°C). Houghton argues that if clouds are convective rather than stratiform in nature, collection processes are likely to be the dominant particle growth modes because of the short time available for particle growth. Also, if there are more ice particles present than assumed by Houghton, the ice-crystal process would be ineffective and collection processes should be the dominant growth modes. There is, in fact, an increasing quantity of experimental evidence which indicates that

¹ Contribution No. 337, Department of Atmospheric Sciences, University of Washington.

² In this study, "mesoscale" refers to features having a horizontal dimension from tens to hundreds of kilometers.

TABLE 1. Observations and measurements made from the research aircraft. Measurements listed in parentheses were not used in this study.

Parameter	Observed or measured by	Range of measurements	Error in measurements	Time constant
General remarks and observations	Flight crew; recorded on taped flight log			
Cloud configurations along aircraft path	Flight observer			
Time	Time code generator (Systron Donner, Model 8220)	h, min, s (IRIG B code)	1 part in 10 ⁵	
Time	Radio WWV; received by Gertsch RHF 1; recorded on taped flight log			
Aircraft position and course plotter	Works off DME and VOR (in house)	80 mi	~1 mi	10 s
(Altitude above terrain)	Radar altimeter (AN/APN22)	0-20,000 ft	±5% of indicated value	
(True air speed)	Differential capacitance pressure sensor (Rosemont Eng. Co., Model 831 BA)	0-±1 psi	~±0.2% full scale (manufacturer's spec.)	
Air turbulence	Differential pressure sensor (Meteorology Research Inc., Model 1120)	0-10 cm ³ s ⁻¹	~±10%	3 s
(Vertical velocity)	Glider variometer (Ball Eng. Co., Model 101-D)			
Pressure altitude	Absolute capacitance pressure sensor (Rosemont Eng. Co., Model 830 BA)	0-15 psi	~±0.2% full scale (manufacturer's spec.)	
(Total air temperature)	Platinum wire resistance (Rosemont Eng. Co., 102CY2CG+414 L Bridge)	-100 to +200°C	~±0.1°C (manufacturer's spec.)	~1 s
Static air temperature	Platinum wire resistance (in house)	-100 to +100°C	~±0.5°C	~1 s
Dew point temperature	Dew condensation type instrument (Cambridge, Model 880)	-40 to +50°C	~+1°C (manufacturer's spec.)	2°C s ⁻¹
Cloud liquid water content	Hot wire resistance (Johnson-Williams)	0.1-2 g m ⁻³ or 0.1-6 g m ⁻³		
(Cloud droplet size distribution)	Keily electrostatic droplet probe			
(Hydrometeor samples)	Metal foil impactor (Meteorology Research, Inc., Model 1220A)	Particles >250 μm in size		
Cloud particle samples, concentrations	Continuous particle replicator (Meteorology Research, Inc., Model 1203D)	>0.1 ℓ ⁻¹		
Ice particle concentrations	Optical polarization counter (in house)	0-100 ℓ ⁻¹		Immediate
(Cloud condensation nuclei)	Optical (light scattering) counter (in house)	0-5000 cm ⁻¹	±10%	1 cycle per 15 s
(Ice nucleus concentrations)	Fast response polarizing technique (Mee Industries)	0.1-10,000 counts per liter		10 s
(Electric field in vertical plane)	Rotary field mill (Meteorology Research, Inc., Model 611)	0 to ±100 kV m ⁻¹	±10%	0.2 s
(Electric field in horizontal plane)	Rotary field mill (Meteorology Research, Inc., Model 611)	0 to ±100 kV m ⁻¹	±10%	0.2 s

many mid-latitude clouds do contain concentrations of ice particles which are several orders of magnitude larger than measurements of ice nuclei would suggest. Braham (1964) and Mossop *et al.* (1967) have observed such high concentrations of ice particles in isolated cumulus clouds, and Hobbs (1973) has reported on extensive measurements which show that high ice particle concentrations are also a very common feature of orographic and frontal clouds over the Cascade Moun-

tains of Washington State. In view of these measurements, and since frontal clouds are usually not purely stratiform in nature but rather a mixture of stratiform and convective clouds, it appears that the microphysics of frontal clouds may be much more complicated than envisaged by the classical ice-crystal process.

Although the importance of mesoscale cloud organization and the complexity of the role of the ice phase in clouds are now well recognized, our physical under-

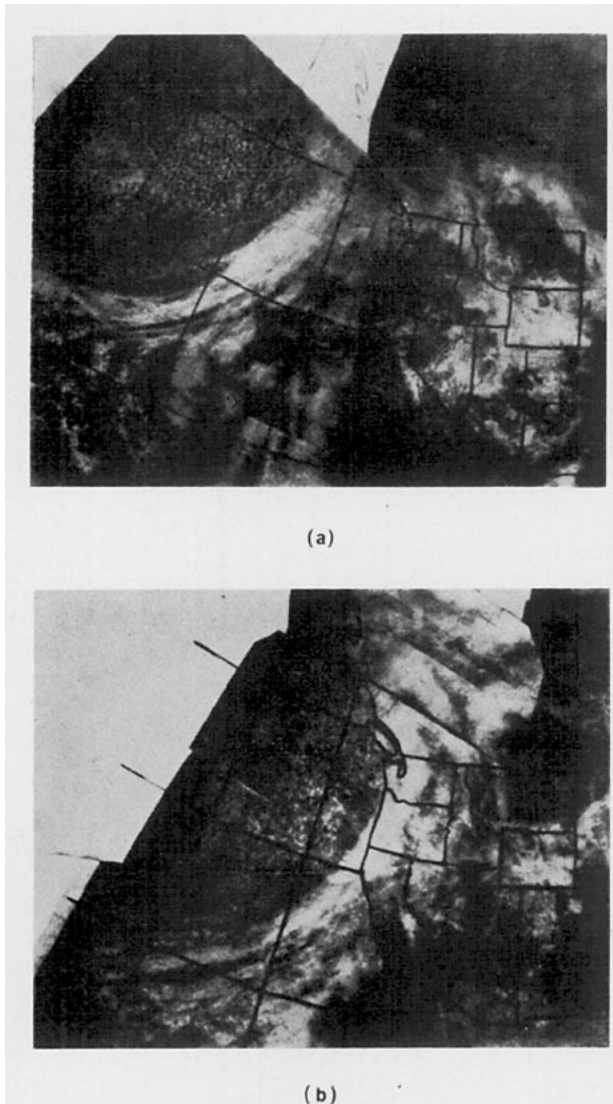


FIG. 1. Satellite cloud photographs of the North Pacific and western coast of North America showing the occluded frontal system (a) approaching the coast at 1000 PST, 15 March 1973, and (b) moving through central Washington at 1000 PST, 16 March 1973.

standing of these aspects of cyclonic precipitation is very rudimentary. Without an adequate understanding of frontal precipitation processes, significant improvements in short-term forecasting are unlikely. As a first step toward obtaining this understanding, field studies are required with measurements encompassing a very broad range of scales: synoptic, meso, cumulus and microphysical. At the University of Washington, we have initiated a series of case studies to investigate the structure of cyclonic storms in the state of Washington over this entire range of scales.

The case described in this paper is the first in this series. It is concerned with an occluded frontal system which moved inland from the Pacific Ocean, across the low-lying Puget Sound Basin of Washington, and then

over the Cascade Range. It is a somewhat unusual case in that the system did not contain a broad region of precipitation ahead of the occluded front, nor did it contain a series of mesoscale precipitation areas. Instead, the precipitation was contained in a single mesoscale band aligned along the front. The dynamical and microphysical structure of this mesoscale cloud band were extensively documented by sequential rawinsonde ascents, a raingage network, and aircraft penetrations. In this paper we describe (i) the overall dynamical structure of the frontal system, (ii) the detailed dynamical and microphysical structure of the frontal cloud band, and (iii) the modification of the frontal dynamics and cloud structure as the system passed over the Cascade Range.

2. Types of data

The dynamical structure of the frontal system was investigated by launching rawinsondes from a single site at intervals of 2–3 h. The rawinsonde station was operated by the Cloud Physics Group of the University of Washington at North Bend, Wash., near the base of the western foothills of the Cascade Range. As the frontal system passed over this location, it did not as yet appear to have been significantly affected by the presence of the Cascades.

Vertical air motions were deduced from the single-station rawinsonde data by two different methods. In each method, it was assumed that the frontal system was approximately two-dimensional and in a steady-state condition in a coordinate system moving with the system. In the first method, it was further assumed that the wet-bulb potential temperature (θ_w) was conserved, which is true for both dry- and moist-adiabatic processes. In this case, the equation for the vertical velocity (ω) is

$$\omega \equiv (U_x - u_x) \frac{\partial \theta_w / \partial x}{\partial \theta_w / \partial p}, \quad (1)$$

where p is the pressure, t time, x the horizontal coordinate perpendicular to the front, U_x the frontal velocity in the x direction, and u_x the wind component in the x direction. This relation was applied between adjacent soundings at vertical increments of 50 mb. Since ω becomes indeterminate for small values of $\partial \theta_w / \partial p$, 0.01 K mb⁻¹ was taken to be the smallest significant value of this gradient in the calculations.

Vertical velocities were also calculated from the rawinsonde data by making the time-to-space conversion described above for the idealized two-dimensional frontal system and then using the mass continuity equation in the form

$$\frac{\partial \omega}{\partial p} = - \frac{\partial u_x}{\partial x}, \quad (2)$$

Eq. (2) was integrated vertically in 50 mb increments

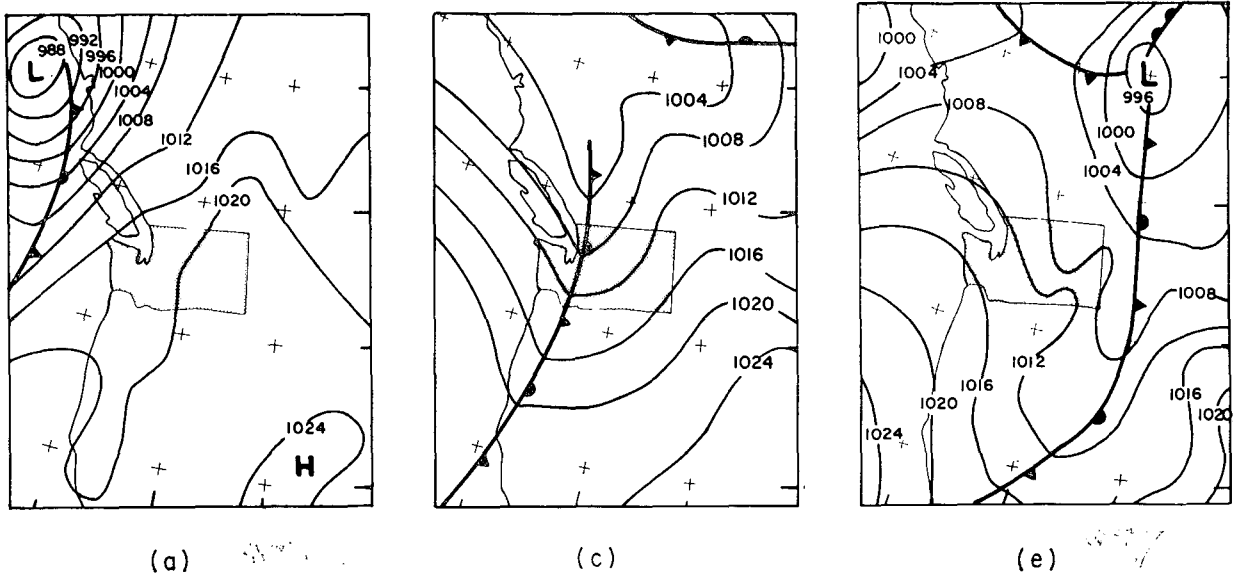


FIG. 2a,c,e. Sea-level pressure analyses (millibars) for 1600 PST 15 March 1973, 1000 PST 16 March, and 2200 PST 16 March, respectively.

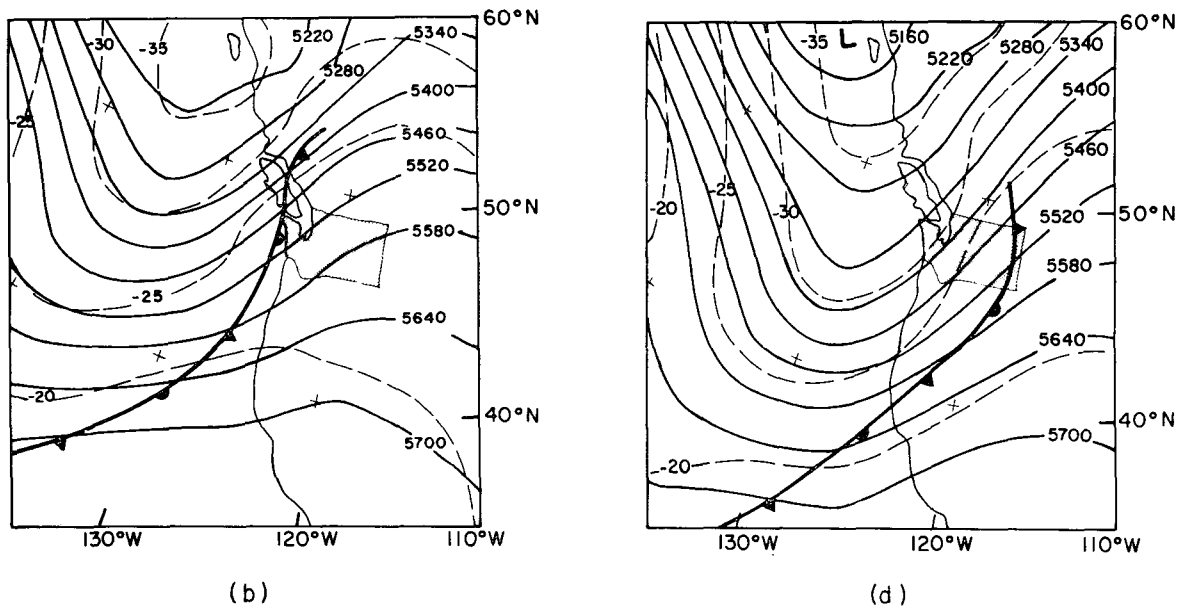


FIG. 2b,d. 500 mb height analysis (meters) and surface frontal position for 0400 PST 16 March 1973 and 1600 PST 16 March, respectively.

assuming that $\omega=0$ at the ground. Since the frontal cloud layer was in the lower troposphere (below 600 mb), accumulation of errors with height in the calculation was not considered to be especially significant in the regions of primary interest.

Cloud microphysical data were obtained with the University of Washington's converted Douglas B-23 research aircraft. Detailed descriptions of the aircraft and its cloud physics instrumentation have been given by Hobbs *et al.* (1971, 1972). The measurements which can be made from the aircraft are summarized in Table

1. The measurements of ice particle concentrations are of particular interest in this study. The two instruments used to measure ice particle concentrations were a continuous Formvar particle replicator and the University of Washington's automatic optical ice particle counter (Turner and Radke, 1973). The smallest particles which can be detected with these two devices are about 3 and 100 μm in maximum dimension, respectively.

Precipitation gages with time resolutions ranging from 15 s to 2 min were operated at ten locations. These data were supplemented by hourly precipitation amounts

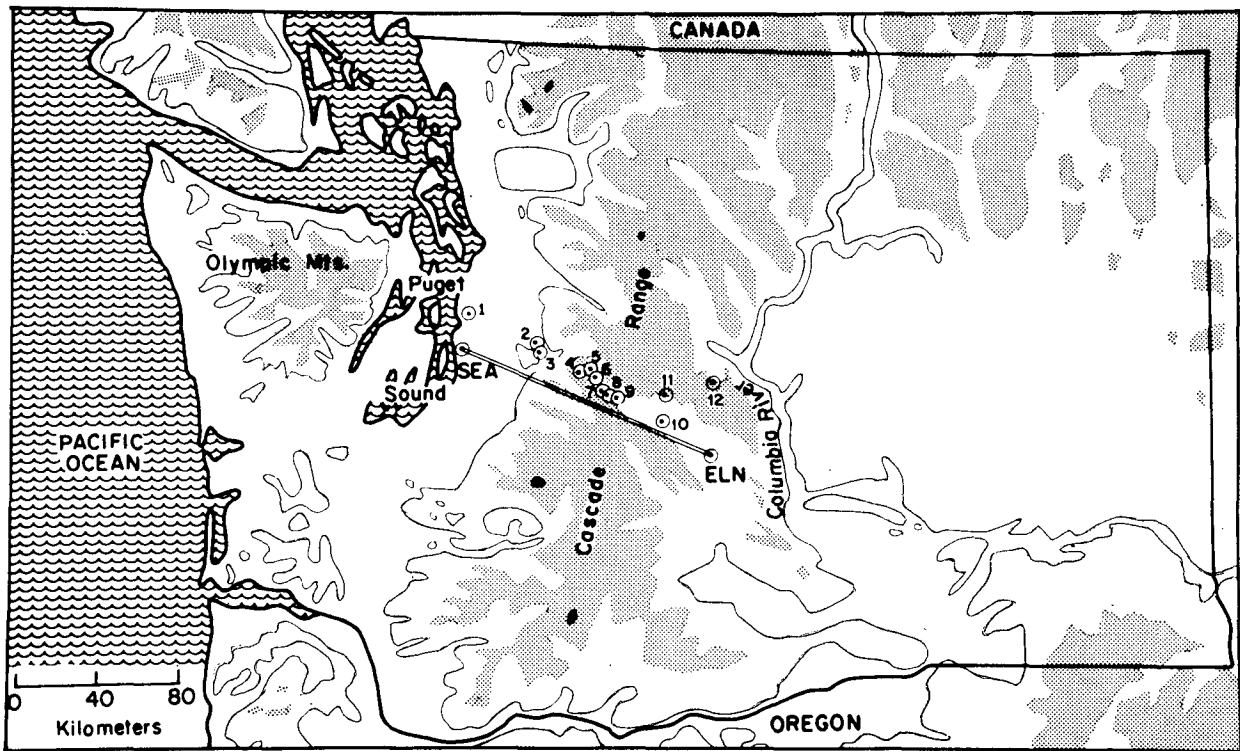


FIG. 3. Topographical map of Washington showing water, land areas above 5000 ft (stippled) and 10,000 ft (black areas), the 1000 ft height contour (thin solid line), the aircraft flight path (double line) between Seattle (SEA) and Ellensburg (ELN), and locations of observing stations operated by the University of Washington: (1) University of Washington, (2) Rawinsonde site, (3) North Bend, (4) Bandera, (5) Snoqualmie Summit, (6) Hyak, (7) Keechelus Lake Dam, (8) Cabin Creek, (9) Kachess Lake Dam, (10) South Cle Elum, (11) Teanaway, (12) Swauk Pass.

from 82 reporting gage stations throughout Washington (NOAA, 1973).

In addition to the above data, satellite photographs and conventional meteorological data were obtained from the National Weather Service.

3. General synoptic and topographical situation

An occluded frontal system moved into western Washington from the Pacific at approximately 0600 (all times Pacific Standard) on 16 March 1973, and progressed across the state during the remainder of the day. Satellite photographs and synoptic maps are shown in Figs. 1 and 2. The front extended southward from a cyclonic center which moved onshore some 1100 km to the north. This low had developed late in the day of 13 March from a frontal wave in the North Pacific located at roughly 40°N , 160°W , and it was still deepening when it reached the coast (Fig. 2a). Although this low became disorganized as it crossed the mountains of British Columbia during 16 March (Fig. 2c), by that evening it had already re-formed to the east of the mountains (Fig. 2e). The frontal system was located on the eastern side of an upper-level trough which passed over Washington on 17 March.

The topography of Washington is characterized by two major mountain systems: the Olympic Mountains in northwestern Washington, and the Cascade Range in central Washington which extends north-south across the entire state. To the west of the Cascades (between the two mountain ranges) is the fairly level and low-lying Puget Sound Basin, while to the east is a vast and quite dry plain. Most of the data used in this study were taken in the area extending from Seattle, in the Puget Sound Basin, eastward across the Cascade Range to Ellensburg, at the foot of the eastern slope of the Cascades. A map of Washington showing the topography, the locations of the ground stations, and the flight path of the research aircraft is shown in Fig. 3. By making several traverses of the Puget Sound and Cascade Range, measurements were obtained from the aircraft in various regions of the frontal system and for different positions of the front in relation to the orography.

4. Positioning of surface front

It was necessary for much of the analysis to have an accurate determination of the motion of the front through Washington. The front, however, was not

always sharply defined at the surface; in particular, the surface pressure trough, wind shifts, and temperature drops often appeared to be somewhat out of phase as the front progressed inland. Since the surface pressure trough was the most clearly defined feature, it was used to indicate the progress of the frontal zone.

Hourly surface analyses from the period the front was passing through western Washington are shown in Fig. 4. The frontal trough lines were located objectively by first fitting a parabola to the three successive hourly pressure observations which bracketed the trough passage at each station and then drawing isochrones of the trough line at hourly intervals. In only one instance did the objectively determined trough position have to be adjusted slightly to agree with the 3 h pressure tendencies reported at 0700 and 1000 PST. The slightly out-of-phase character of the trough and wind-shift lines is most clearly indicated by examining the hourly sequence of observations at Olympia (OLM) in Fig. 4.

By plotting the times of the frontal trough passage versus the longitude of the stations in Washington, it was found that the eastward velocity of the frontal zone from the Pacific Coast through the Cascade Mountains was very nearly constant at 37 km h⁻¹.

5. Vertical structure of the frontal system

a. Cross sections

Vertical time sections through the frontal zone and the adjoining air masses were constructed from the serial rawinsonde data. The time section of temperature, wind direction and wind speed is shown in Fig. 5a. The time sections of relative humidity, wet-bulb potential temperature, and the wind components along and perpendicular to the direction of frontal motion are shown in Figs. 5b–5e. The horizontal axes are labelled in hours after the surface frontal trough passage and are converted to a west–east distance scale using the observed eastward frontal velocity of 37 km h⁻¹.

b. The occluded front

The occluded front in Fig. 5a is located at the leading edge of a zone of strong horizontal temperature gradient which extends from upper levels downward into the surface pressure trough. The vertical wind pattern in Fig. 5a shows that the air just below the front was characterized by cold advection (winds backing with height) while the air just above was characterized by nearly neutral or warm advection (winds veering with height).

In Fig. 5b it is seen that the cold air mass behind the occluded front was bounded by a zone of strong gradient of wet-bulb potential temperature (θ_w). In Fig. 5c the occluded frontal surface coincides with a maximum of relative humidity.

c. Pre-frontal structure

A well-defined, warm-frontal surface did not exist ahead of the occlusion. Instead, the weakly-packed wet-bulb potential temperature isotherms in the pre-frontal region (Fig. 5b) displayed a pronounced wavy pattern. When the time axis of the cross section is converted to a distance scale, the distance between these waves is found to be on the order of 220 km. This structure is very similar to that observed by Elliott and Hovind (1965) in occlusions off the coast of California, storms which are similar in origin to the one studied here.

d. Pre-frontal surge

Among the alternating tongues of low and high wet-bulb potential temperature air seen in the wavy structure ahead of the occluded front in Fig. 5b, was a particularly pronounced tongue of low- θ_w air located aloft immediately ahead of the occluded front. The position of this low- θ_w tongue is very similar to that observed by Kreitzberg and Brown (1970). Their terminology is adopted in referring to this feature as a “pre-frontal surge.” In the present case, the pre-frontal surge apparently had some frontal characteristics as it was bounded by a discontinuity in the temperature and wind gradients (see Figs. 5a and 5e).

Kreitzberg and Brown (1970) argued that the air in pre-frontal surges is originally located within the cold air mass, and breaks away during a postulated frontal evolutionary process. An alternative explanation is that the air in this layer may have been subtropical in origin, having travelled northward just ahead of the approaching front.

In an effort to investigate the origin of the air in the pre-frontal surge, a trajectory was computed using the 700 mb winds from the upper air station at Quillayute on the Washington coast and geostrophic winds based on available 700 mb height contour analyses over the Pacific Ocean (see Fig. 6). Although the computed trajectory appears to emanate from behind the surface frontal position, the uncertainty in the map analyses over the ocean is too great to draw any definite conclusion about which side of the front the trajectory actually came from.

e. Low-level high- θ_w zone

A strong, closed maximum of wet-bulb potential temperature was observed near the surface in the occluded frontal zone (Fig. 5b). This narrow zone of high- θ_w air is also evident in the hourly maps shown in Fig. 4; it progressed inland from the Pacific coastline and maintained a constant orientation along the frontal trough line. The translation of this high- θ_w zone over the rawinsonde site apparently produced the maximum of θ_w in the surface frontal zone in Fig. 5b. The high values of θ_w at the rawinsonde station were probably enhanced by diurnal heating (the maximum value of θ_w at the

rawinsonde site occurred at 1030). However, the low-level, high- θ_w zone cannot be fully accounted for in this way since the feature was observed on the coastline of Washington at about sunrise and the maximum of θ_w was noted in hourly reports at all western Washington stations as a maximum in dew point as well as temperature.

The origin of the air in the high- θ_w zone was investigated by constructing trajectories from surface winds reported in western Washington and Oregon and winds estimated from surface pressure analyses over the Pacific Ocean. The calculated trajectories are shown in Fig. 7. The generally southerly and south-southwesterly trajectories of air parcels arriving in the high- θ_w zone (B and C in Fig. 7) suggest that these parcels had a generally warm maritime character; whereas immediately to the west, colder maritime air was arriving from the west (D in Fig. 7). On the east, the high- θ_w zone was bounded by air with continental trajectories such as A in Fig. 7. Evidently, the high- θ_w zone seen in Fig. 4 was a narrow wedge of warm maritime air wedged between cold maritime air to the west and dry continental air to the east.

The occurrence of low-level flows of high- θ_w air in the vicinity of occluded frontal zones over California was noted by Elliott and Hovind (1965). Browning (1971) and Harrold (1973) have described "conveyor belts" of warm, moist air in frontal systems over the North Atlantic Ocean. Browning and Pardoe (1973) detected low-level, high- θ_w jets ahead of cold fronts over the North Atlantic Ocean.

While the southerly flow in the high- θ_w zone seen in Fig. 4 was not marked by a maximum in the wind component parallel to the front in the relevant sounding taken through the high- θ_w zone (Fig. 5e), the surface synoptic data from western Washington suggest that a weak, southerly jet did occur in the high- θ_w zone (Fig. 4d presents the clearest data in support of this). However, this high- θ_w flow appears to be of a different nature than those reported by previous investigators. In the present case the air parcels in the southerly flow were being overtaken quite rapidly by the approaching front (see Fig. 7b). This aspect of the high- θ_w flow is unlike the "conveyor" belt described by Browning and his colleagues in which parcels of air apparently flow parallel to the front in a *relative* sense for long periods of time.

It should be noted, however, that the airflow pattern in the present case may have been different while the system was passing over the Pacific Ocean than it was as the front moved inland. The strong cross-isobaric flow in the high- θ_w zone seen in Fig. 4 suggests that the flow was influenced by frictional effects associated with topography as the frontal system moved inland. Over the ocean there would have been a broad region of warm maritime air ahead of the front and surface frictional effects would have been minimal. In the oceanic

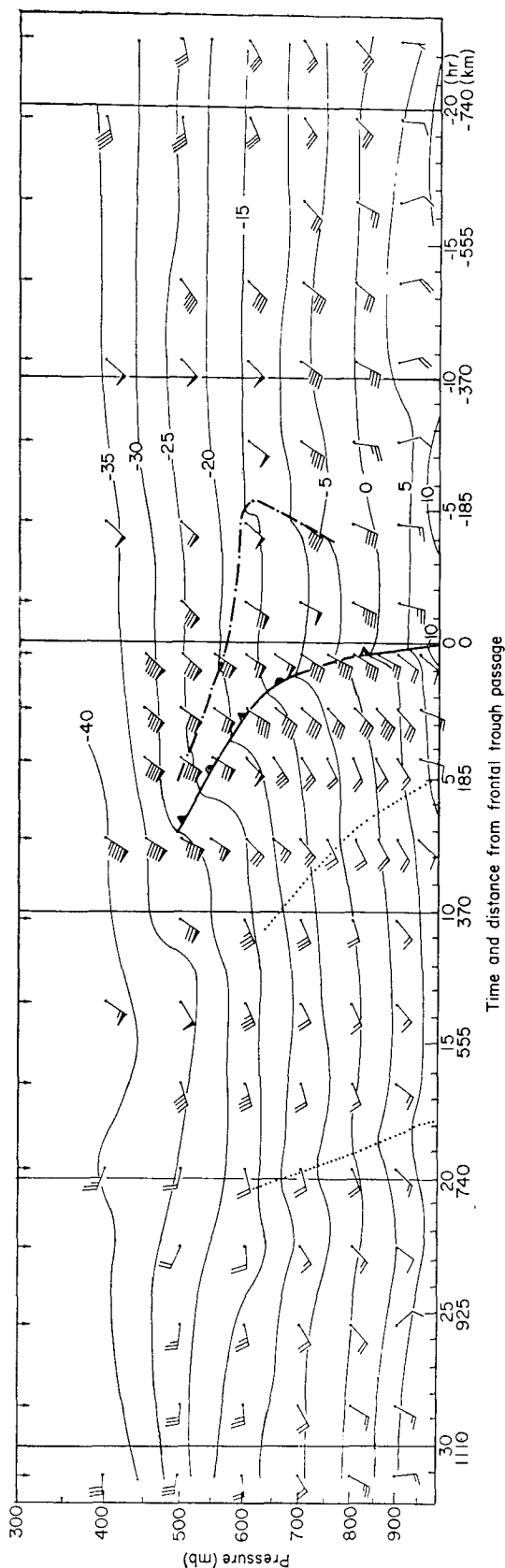


Fig. 5a. Vertical cross section of temperature ($^{\circ}\text{C}$) and winds measured by serial rawinsondes. Time-to-space conversion is based on frontal speed of 37 km h^{-1} . A full wind barb has a value of 10 kt, a pennant 50 kt. Other symbols represent the pre-frontal surge (dash-dotted line), the occluded front, the post-frontal surge (dotted line), high wet-bulb potential temperature tongues (dotted lines). Arrows at top indicate sounding times.

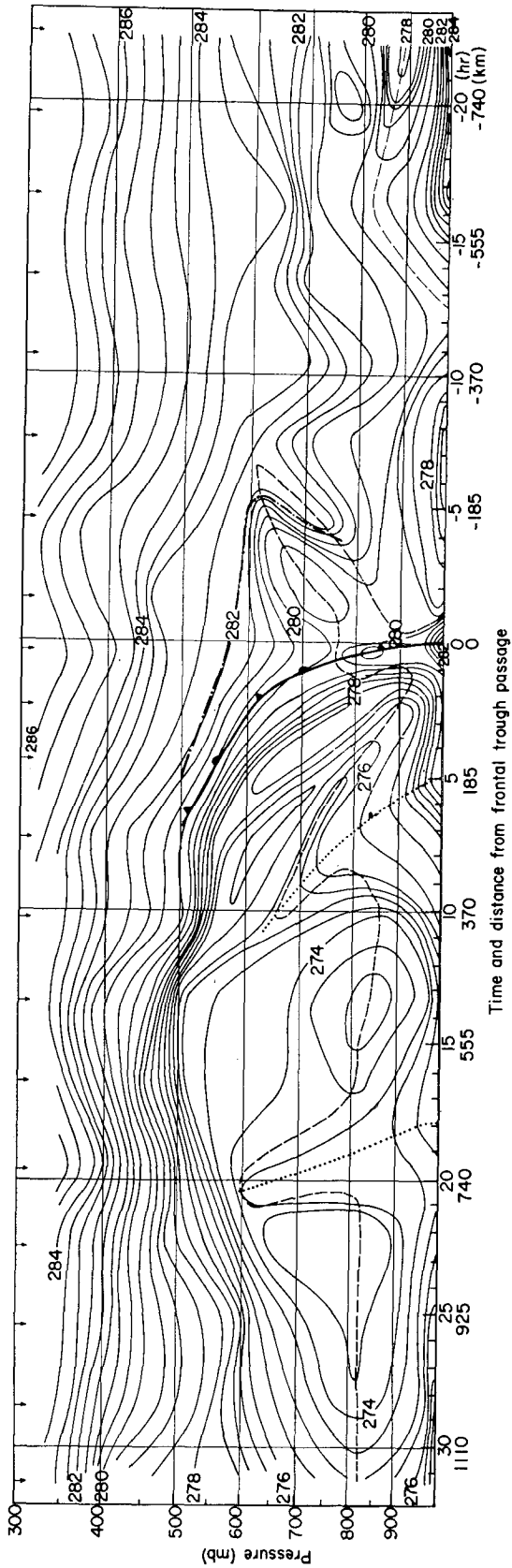


FIG. 5b. Vertical cross section of wet-bulb potential temperature ($^{\circ}\text{K}$). Region enclosed beneath dashed line was potentially unstable. Other symbols are as in Fig. 5a.

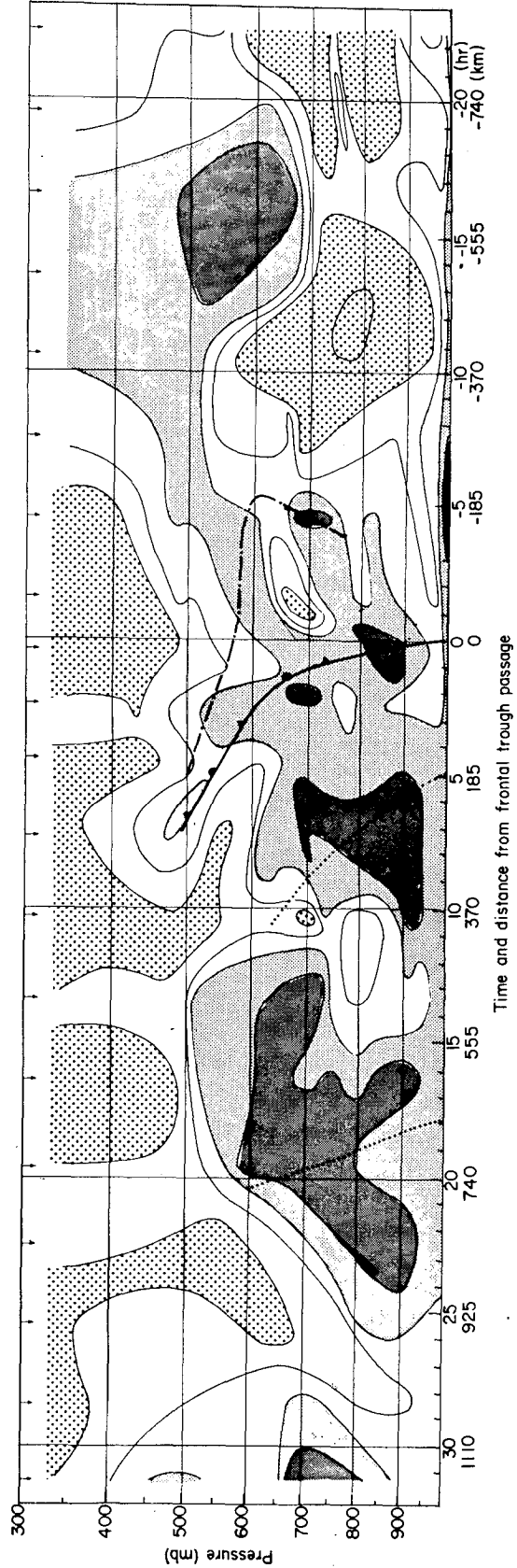


FIG. 5c. Vertical cross section of relative humidity (with respect to liquid water). Regions of relative humidity greater than 90% are indicated by dark shading, between 70 and 90% by light shading, and less than 30% by stippling. Other symbols are as in Fig. 5a.

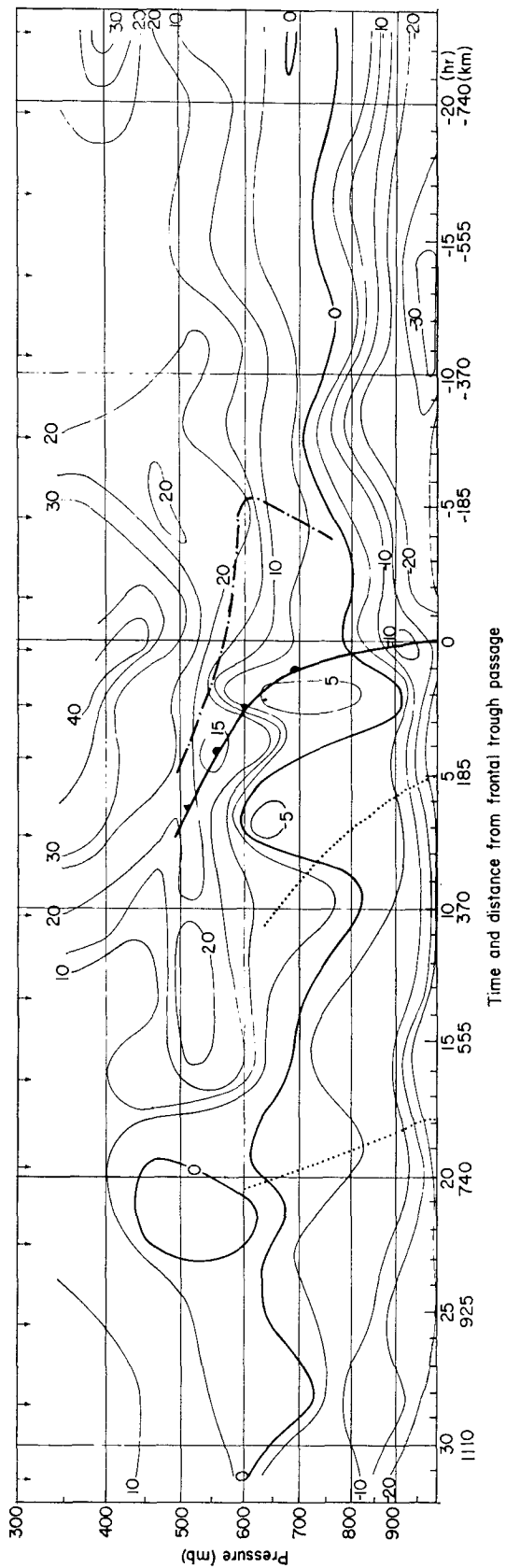


Fig. 5d. Vertical cross section of wind normal to front. Values are in knots with the speed of the frontal system subtracted from them to represent the flow relative to the system.

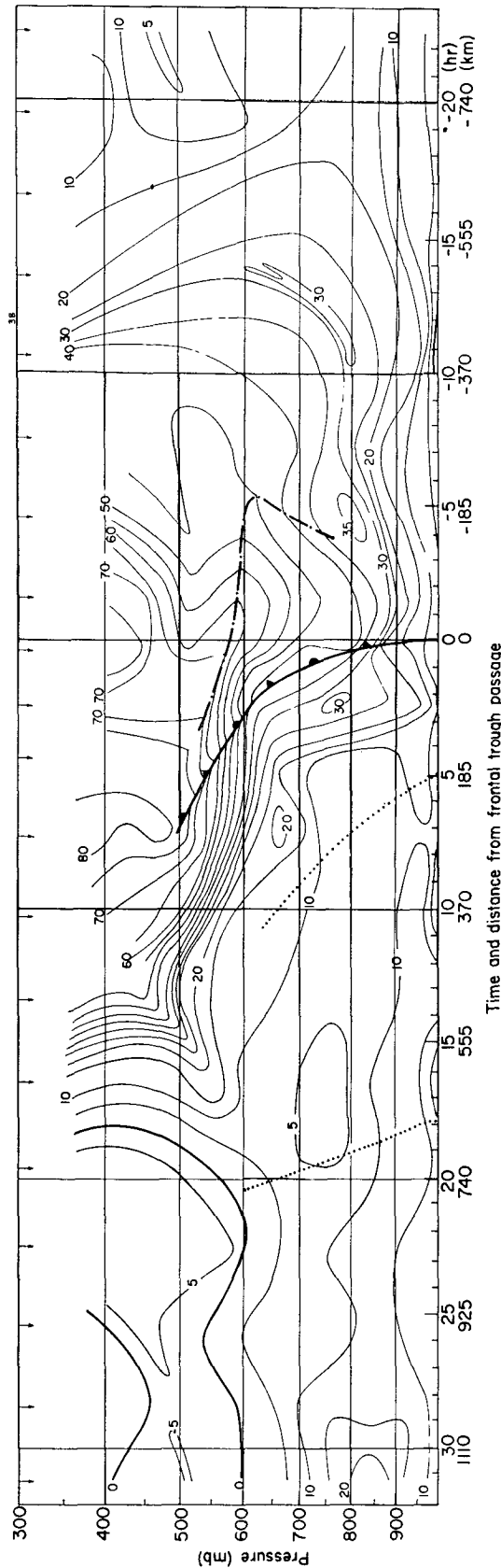


Fig. 5e. Vertical cross section of wind parallel to front. Values are in knots.

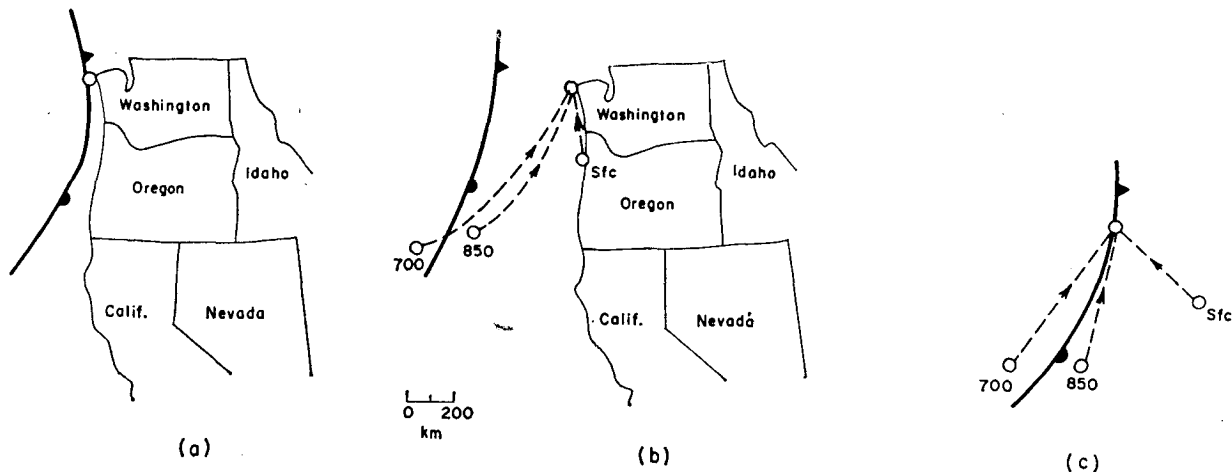


FIG. 6. Position of surface front and a column of air (open circle) near the northwest tip of Washington at 0400 PST 16 March 1973 (a); trajectories of air parcels at surface (Sfc), 850 mb and 700 mb levels during 12 h prior to their arrival at northwest tip of Washington for surface front at 1600 PST 15 March 1973 (b); same trajectories as in Fig. 6b in a coordinate system moving with the front (c).

environment a broad low-level jet of high- θ_w air of the type described by previous investigators could have developed. As the front move inland, however, the pre-frontal region began to be characterized increasingly by continental air, and the narrow high- θ_w zone seen in Fig. 4 was probably the last vestige of warm marine air encountered by the front before the system began to interact with drier continental air from east of the Cascade Range.

f. Post-frontal structure

Two mesoscale tongues of high- θ_w air occurred in the cold air mass well behind the occluded front; they are denoted by dotted lines in Figs. 5a-5f. Their structure in the wet-bulb potential temperature field is qualitatively similar to that of the high- θ_w tongue associated with the occluded front, except that the later tongues are broader and more diffuse, each covering a period of 3-5 h at the rawinsonde site. The axis of each warm

tongue was followed by a secondary surge of low- θ_w air bounded by a relatively strong gradient of wet-bulb potential temperature (see Fig. 4b), thus suggesting that a weak secondary frontal structure existed behind the primary, occluded front.

Post-frontal, warm- θ_w tongues were noted by Kreitzberg and Brown (1970) and were identified with a secondary frontal structure.

6. Cloud dynamics

a. Vertical velocities and streamlines

The region ahead of the occluded front shown in Figs. 1 and 2 was devoid of any precipitation except in a narrow mesoscale band aligned along the front itself. To study the airflow in this precipitation band, vertical velocities were computed by the isentropic and mass-conservation methods [Eqs. (1) and (2)] and added to the horizontal wind components relative to the front

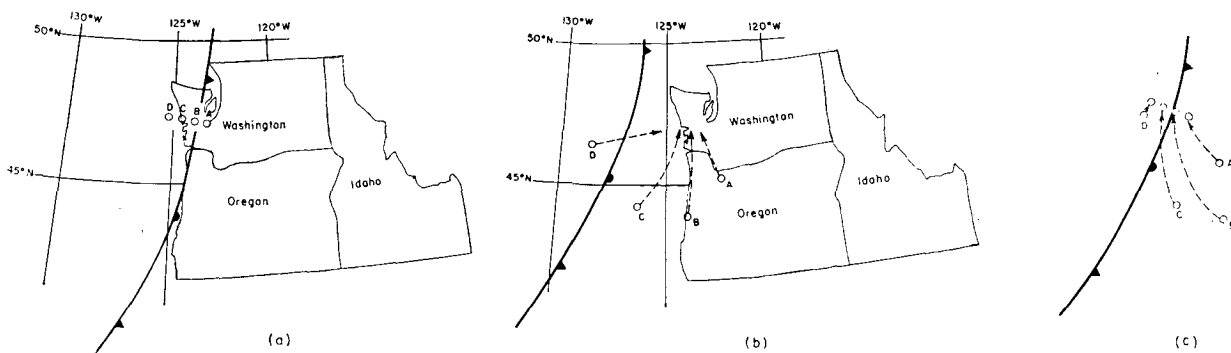


FIG. 7. Position of surface front and air parcels (A-D) at 0700 PST 16 March 1973 (a); trajectories of air parcels (A-D) during 12 h prior to 0700 PST 16 March 1973 for surface front at 1600 PST 15 March 1973 (b); same trajectories as in Fig. 7b in a coordinate system moving with the front (c).

to obtain streamline patterns in the cross-section plane. The resulting flow patterns are shown in Figs. 8 and 9. (In Fig. 8 vertical velocities computed by the isentropic method have been omitted at grid points for which the vertical gradient of θ_w in a 50 mb layer was small enough to make ω indeterminate. Dashed vectors indicate where vertical velocities were computed using a grid spacing larger than 50 mb.)

In general, the two vertical velocity and streamline patterns in Figs. 8 and 9 agree quite well, the main difference being the lifting behind the front which appears only in the mass continuity calculations (Fig. 9). Below the 850 mb level, a flow through the front is indicated in both Figs. 8 and 9 because of the strong relative horizontal flow toward the front in this layer (10–15 kt). Flow through fronts at low levels has been noted previously and it has been suggested that when this occurs the temperature contrast across the front is maintained by mixing of the cold air mass into the boundary layer (e.g., Saucier, 1955, p. 190).

Hourly precipitation amounts in the Puget Sound Basin (to be discussed in Section 8) indicate that the average rainfall rate in the frontal band was approximately 1 mm h^{-1} . The vertical velocity required to produce this rainfall rate is 28 mb h^{-1} (assuming that condensation occurred as a result of uniform lifting between the 900 and 600 mb levels). This rate of ascent in the frontal cloud agrees very well with the vertical velocities computed isentropically (Fig. 8) and from

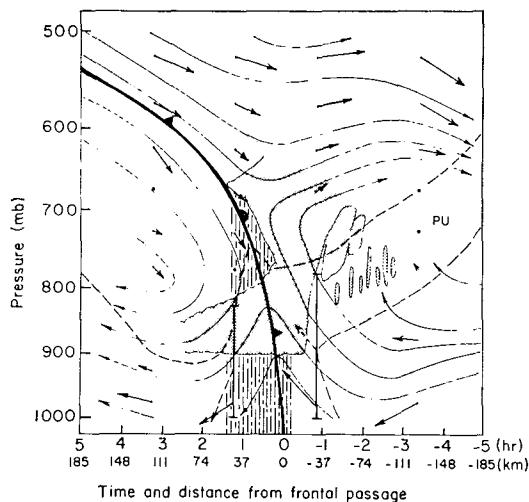


FIG. 8. Streamlines relative to front with vertical velocities computed from conservation of wet-bulb potential temperature. Clouds (stippled areas) and precipitation (vertical hatching) are as observed from aircraft and ground. Potentially unstable air (PU) is enclosed by the dashed lines. Vectors show displacement of a parcel in 1 h at its computed velocity with vertical component in millibars and horizontal component in kilometers. Dashed vectors were plotted when vertical grid increments (shown by bars) larger than 50 mb were used in calculating the vertical velocity. Dots show grid points for which a reliable vertical velocity could not be calculated because of a small vertical gradient of wet-bulb potential temperature.

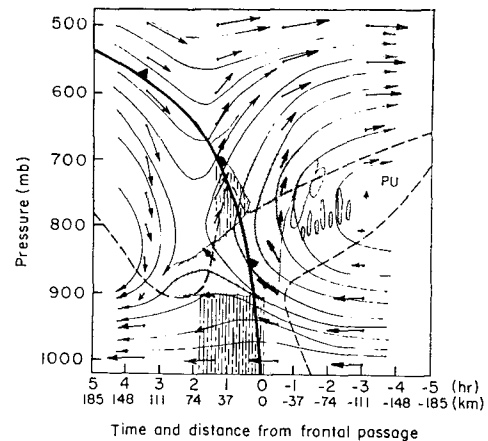


FIG. 9. As in Fig. 8 except for vertical velocities computed from two-dimensional mass continuity equation. Discussion relevant to dashed vectors and dots in legend to Fig. 8 is not applicable.

mass continuity (Fig. 9) which ranged from about -20 to -50 mb h^{-1} (or 6 to 14 cm s^{-1}) in the region just ahead of the front.

b. Airflow relative to observed clouds

In Figs. 8 and 9, the cloud configuration is shown as it was sketched onboard the research aircraft during one flight through the frontal cloud band. At the time of this flight, the front was moving across the Puget Sound Basin and approaching the rawinsonde site in the foothills of the Cascades. Since the cloud mass observed from the aircraft was not located directly over the rawinsonde site, the cloud sketch has been projected onto the cross section so that the clouds are in their proper position with respect to the occluded front. Minor vertical adjustments were made to account for differences in terrain height between the rawinsonde station and the aircraft location.

In general, there is very good qualitative agreement between the air motion and cloud patterns shown in Figs. 8 and 9. The region of maximum lifting coincides precisely with the most extensive frontal cloud zone. The small cumulus clouds ahead of the main cloud band in Fig. 8b were located in the shallow layer of potential instability ahead of the front. The instability was apparently being released by the upward motion in that region. The observed forward slope of the main frontal cloud is consistent with the observed horizontal winds which were moving faster than the front aloft and slower at low levels. The clear wedge observed on the cold side of the frontal cloud apparently reflects the intrusion of dry subsiding air from the west into the frontal zone. The tendency of the rainfall to be located behind the surface front is consistent with the general horizontal motion of air parcels from right to left in the lower portion of the frontal cloud shown in Figs. 8 and 9. Condensation apparently occurred first in rising

air parcels on the leading edge of the frontal clouds. Precipitation-size particles developed as the air moved back toward the cold air mass (either above the frontal zone or possibly through it at low levels) and were deposited behind the surface frontal position.

c. Convective nature of the frontal band

There is evidence that the frontal cloud band was partly convective in nature. The lifting of the deep layer of potentially unstable air ahead of the front should have resulted in unstable ascent above the condensation level (see Fig. 8). A comment in the aircraft log referring to the option of flying through or around the frontal clouds at the 700 mb level implies that the cloud band at that level was not actually uniform along the front, but instead consisted of irregular towers. In another pilot report made near Seattle less than 1 h after the frontal trough passage, the tops of the clouds were reported to be at the 2.4 km (750 mb) level, with scattered buildups to 3.4–3.7 km (650 mb).

From the rather slow mean ascent rate of 6–8 cm s⁻¹ computed above it is inferred that convection within the frontal band must have been concentrated in relatively narrow updraft zones. Cloud microphysical data, discussed below in Section 7, suggest that the active convection was in fact concentrated in a narrow zone on the leading edge of the large frontal cloud.

The circulation in the mesoscale frontal band was similar in some respects to that observed in organized convective systems such as the severe thunderstorms described by Newton (1963) or the organized tropical convective systems described by Zipser (1969). The widths of these cloud systems are about 50 to 100 km, the same order as that of the frontal cloud band in the present study. The dynamical structures of organized convective systems are such that they are perpetuated for many hours. In the present case, the moisture and potential instability of the frontal cloud were apparently continually replenished by the low-level inflow of high- θ_w air below the 800 mb level, and lifting to condense the moisture and release the instability was continually provided by the advance of the cold air mass. This lifting may have been supplemented by a precipitation-induced downdraft spreading under the updraft as it does in other organized convective systems. In Fig. 8 the downdraft and precipitation zones do appear to coincide. However, this feature is not seen in Fig. 9 which shows the vertical velocities deduced from the two-dimensional mass-continuity equation.

Browning and Harrold (1970) have also described air motions in a frontal cloud which are similar to those of an organized convective system.

d. Cloud moisture supply

The maintenance of the moisture supply for the frontal cloud can be understood by first noting from Fig. 6 that the air which flowed into a vertical column

located over the Washington coast near the leading edge of the frontal cloud did so along trajectories emanating from the south at the surface and from the south-southwest at 850 mb. Viewed in a coordinate system moving with the front, these air parcels moved toward the front (Fig. 4b). From the relative streamlines shown in Figs. 8 and 9, it is evident that this low-level relative flow toward the front must have supplied much of the moisture for the frontal cloud. The net horizontal convergence of water vapor below the 800 mb level, due to the flow perpendicular to the front, was computed from the sounding data obtained 2 h before and 2 h after the frontal trough passage and was found to have been 4.0×10^4 g s⁻¹ (for a 1 m length of the frontal band). If this moisture was deposited uniformly over a band 80 km wide (the observed average width of the frontal rainband) as fast as it converged, the rainfall rate would have been approximately 1.5 mm h⁻¹. The observed average rainfall rate in the frontal band as it passed over the Puget Sound Basin of western Washington was approximately 1 mm h⁻¹.

Moisture flux calculations further show that the component of the airflow parallel to the front in the moving coordinate system could not have supplied a significant amount of moisture to the frontal cloud. The moisture of the frontal cloud was therefore almost completely maintained by the relative flow of moist air toward the front at very low levels as generally northward moving parcels were continually being overtaken by the eastward moving front.

7. Cloud microphysics

a. General pattern

In Fig. 10, the cloud dynamics serve as a framework for examining the cloud microstructure. The streamlines are the same as in Fig. 8. Microphysical quantities shown in the figure include cloud liquid water content, ice particle concentration, maximum ice particle size, predominant ice crystal type, and degree of ice particle riming. Zones of turbulence encountered by the aircraft are also indicated.

As noted in Section 2, ice particle concentrations were determined by two techniques: Formvar replication and optical detection. The pattern of ice particle concentrations indicated in Fig. 2 and all subsequent figures was arrived at by combining the information from these two methods. The Formvar samples were obtained only intermittently, as shown in Fig. 10, whereas the optical measurements were made continuously. The particular version of the optical ice particle counter in use during this investigation was not rigorously calibrated; however, its readings were found to be well correlated with the ice particle concentrations deduced from Formvar samples. The latter were therefore used to calibrate roughly the optical measurements which could then be used to indicate the detailed variations of ice particle concentration along each flight path.

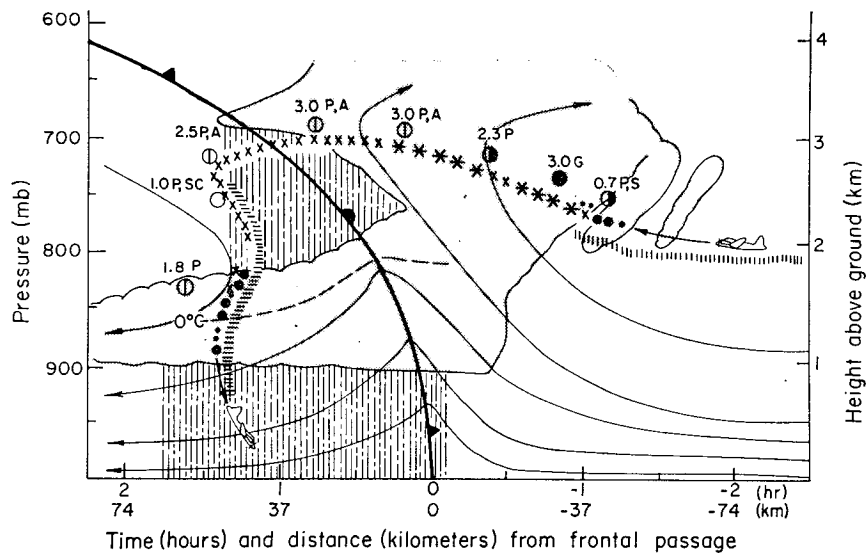


FIG. 10. Cloud microstructure in relation to airflow and front. Continuous cloud microphysical measurements shown in Figs. 10–13 include: cloud liquid water content (\bullet , 0.1 to 0.2 g m^{-3} ; \bullet , $>0.2 \text{ g m}^{-3}$), ice particle concentration (\times , $<45 \text{ l}^{-1}$; $*$, 45 to 95 l^{-1} ; circled asterisk, $>95 \text{ l}^{-1}$). Data from Formvar replicas obtained along routes include: maximum particle size (mm), ice particle types (N, needles and long columns; P, plate-like; S, stellar; SC, short columns, AC, assemblages of columns; SP, assemblages of side planes; A, aggregates; G, graupel; H, hail), and degree of riming (O, none; \odot , light; \ominus , moderate; \bullet , heavy). Turbulence zones are indicated by short dashes along flight path.

The deduction of ice particle concentration from Formvar samples is a difficult problem, and the methods used in this study are discussed in the next section.

It is seen from Fig. 10 that at the flight level of the aircraft the main body of the frontal cloud was composed primarily of ice particles, except within the high-level cumuliform clouds at the forward edge of the main cloud mass and in the lower precipitating cloud deck behind the front. The maximum ice particle size in each sampled volume of the upper part of the frontal cloud was fairly constant. The degree of riming, on the other hand, showed a marked decrease as the aircraft progressed from the liquid water zone on the leading edge of the frontal cloud to the trailing edge of the cloud mass. The region of high riming and liquid water content on the leading edge was also marked by increased turbulence. This combination of factors suggests that this region was the most convectively active part of the frontal cloud.

Most of the ice particles collected during the aircraft flights were irregular in shape. The types which could be identified are indicated in Fig. 10. The possible nucleation temperatures of the identified crystal habits (according to Magono and Lee, 1966) range from -10 to -20°C for the plates and stellars (P and S in Fig. 10) and from -10 to -25°C for the occasional short columns (SC in Fig. 10). The lowest temperature noted at flight level when particle samples were collected was -9.6°C . All of the particles with identifiable habits therefore originated above the flight level of the air-

craft. That is, they were falling through this level as opposed to being transported upward by updrafts. This result is consistent with the average cloud updraft speeds of 6 to 14 cm s^{-1} computed in Section 6a, since the terminal fall velocities of the larger crystals would have been as large as 50 cm s^{-1} (Locatelli and Hobbs, 1974). However, this does not rule out the possibility that some of the irregularly-shaped ice particles or graupel, for which the nucleation temperature is not known, may have been carried upward at some time during their lives by locally intense cumulus-scale updrafts such as were apparently occurring near the leading edge of the frontal cloud.

An interesting feature in Fig. 10 is the precipitation of ice particles from the upper cloud layer into the lower cloud deck behind the front. The “releaser-spender” (or, to use the more common terminology, “seeder-feeder”) process described by Bergeron (1950) may thus have been an important factor in the growth of precipitation in this frontal system.

b. Ice particle concentrations

Observed concentrations of ice particles have received much attention in the last few years as several researchers have reported concentrations which are orders of magnitude larger than ice nucleus concentrations measured at similar temperatures (e.g., Braham, 1964; Mossop *et al.*, 1967; Hobbs and Atkinson, 1975). In the presence of such high concentrations of ice par-

TABLE 2. Ice enhancement ratio R for ice particle concentrations estimated by different counting methods and for ice nucleus concentrations given by Eq. (3) at various ΔT 's.

ΔT (°C)	Lower limit of R	Best esti- mate of R	Value of R using counting method of Hobbs <i>et al.</i> (1972)
10	5×10^3	5×10^4	5×10^5
20	5	5×10	5×10^2
26	$5 \times 10^{-1.5}$	$5 \times 10^{-0.5}$	$5 \times 10^{0.5}$

ticles, Bergeron's (1935) "ice crystal process" would be ineffective as a particle growth mechanism. The possible occurrence of anomalously high concentrations of ice particles was investigated for the frontal cloud band studied here.

Before examining the results of this investigation, it should be noted that ice particle concentrations inferred from Formvar samples are very sensitive to the criteria adopted in counting the replicated particles. However, by making counts under different sets of assumptions, limiting values of the concentrations can be determined.

Of the various counting procedures which may be adopted, the most conservative estimates of ice particle concentrations are obtained by counting only regularly-shaped ice particles which have been replicated intact, and by counting fragmented blotches of ice particles as single particles. A less restrictive technique, described by Hobbs *et al.* (1972), is to count all the ice particles collected (irregular as well as regular) unless they were obviously produced by fragmentation during collection. Careful comparisons of these two methods by our group have shown that for particle concentrations of the order of those encountered during the flight shown in Fig. 10, the second counting method gives estimates which are generally about two orders of magnitude larger than the conservative estimate. The latter is hereafter referred to as the lower limit concentration. The ice particle concentrations indicated in Fig. 10 were obtained by counting the crystals first using the method described by Hobbs *et al.* (1972) then lowering the count by one order of magnitude to give our best estimate of the true concentration. While these best estimates give concentrations on the order of 50 to 100 ℓ^{-1} , the values could have been an order of magnitude greater.

Since the optimum concentration of ice particles for growth of particles by deposition from the vapor phase is about 1 ℓ^{-1} , the classical ice-crystal process would not have been very effective in the frontal cloud shown in Fig. 10. However, the prevalence of rimed ice particles and aggregates found along the flight path of the aircraft suggests that collection processes were important in producing precipitation-size particles.

The observed ice particle concentrations have been compared with ice nucleus concentration N computed

from the relationship

$$N = 10^{(\Delta T - 20)/4}, \quad (3)$$

where N is the concentration of active nuclei per liter at a supercooling ΔT (expressed in degrees Celsius). This relation predicts ice nucleus concentrations which are in the center of the measured values described by Fletcher (1962, p. 241).

Following Hobbs (1969) the ratio of the observed ice particle concentration to the assumed ice nucleus concentration [as given by Eq. (3)] is referred to as the "ice enhancement ratio" (R). Values of R for a typical value of the ice particle concentration found along the flight path shown in Fig. 10 are listed in Table 2. The values of ΔT used in these computations are based on the nucleation temperatures of the crystal habits noted along the flight path in Fig. 10 and on the cloud top temperature (-26°C) estimated from the rawinsonde data. The values 10°C and 20°C for ΔT in Table 2 correspond to the highest and lowest possible nucleation temperatures for plate-like or stellar crystals which were found in all but one sample, while $\Delta T = 26^\circ\text{C}$ corresponds to the cloud top temperature and to the lowest nucleation temperature for the occasional short columns found in one sample.

The values of R in Table 2 suggest that ice enhancement may have been present in the frontal cloud, although the evidence is not conclusive. If most of the sampled ice particles were nucleated between -10 and -20°C , as is suggested by the prevalence of plates and stellars, then the ice enhancement ratio would have been somewhere between 5×10^4 and 50 according to our best estimate of the ice particle concentrations (see Table 2). However, if the majority of the ice particles sampled were actually nucleated near cloud top (-26°C), then there was no ice enhancement.

Although unusually high ice particle concentrations have been observed by several researchers (as noted previously), no physical process has yet been described which adequately accounts for them. It has been noted, however, that anomalously high ice particle concentrations do not appear to be found in clouds which have existed for less than about 10 min [see reviews by Mossop (1970) and Hobbs (1973)]. This time scale is consistent with our knowledge of the frontal cloud system portrayed in Fig. 10. Indeed, because of its quasi-steady nature, this cloud system could have existed for several hours before it was penetrated by the aircraft.

Although the evidence for ice enhancement is inconclusive in this particular frontal cloud, our studies are revealing that ice enhancement in various types of Pacific Northwest cloud systems is not uncommon. Further case studies of frontal systems, with detailed documentation of the cloud dynamics and microphysics, are evidently required to clarify the role of cloud ice in the precipitation processes of frontal clouds.

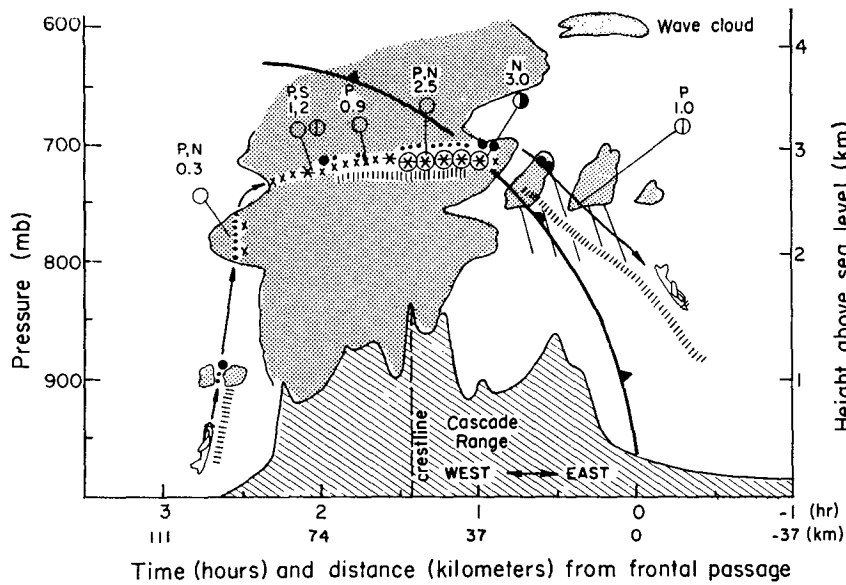


FIG. 11. Cloud configuration and microstructure in relation to front and orography as surface front crossed the leeward slope of the Cascade Range. For key to symbols, see legend to Fig. 10.

8. Orographic effects

a. Cloud structure and microphysics

In this section, we examine the changes in the frontal system as it passed over the Cascade Range, which runs north-south through central Washington. By examining changes in the cloud configuration and microstructure as the front moved across the Cascade Range, it is possible to deduce various effects of the mountains on the dynamics of the frontal system. These effects appear to be of two kinds: the alteration of the vertical

motion pattern due to forced orographic lifting and subsidence, and the blocking of the horizontal wind by the mountain barrier.

During the passage of the frontal system the winds above the 930 mb level all had a westerly component. Consequently the western side of the Cascade Range was the windward slope of the range and the eastern side was the leeward slope.

Figs. 11-13 illustrate the changes in cloud structure which occurred over the Cascade Range. These figures

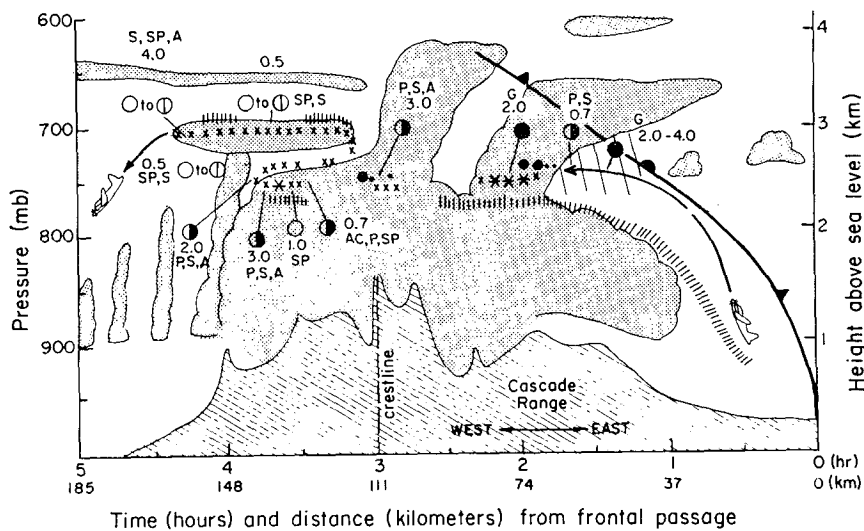


FIG. 12. Cloud configuration and microstructure in relation to front and orography approximately 1 h after the front had crossed Cascade Range. For key to symbols see legend to Fig. 10.

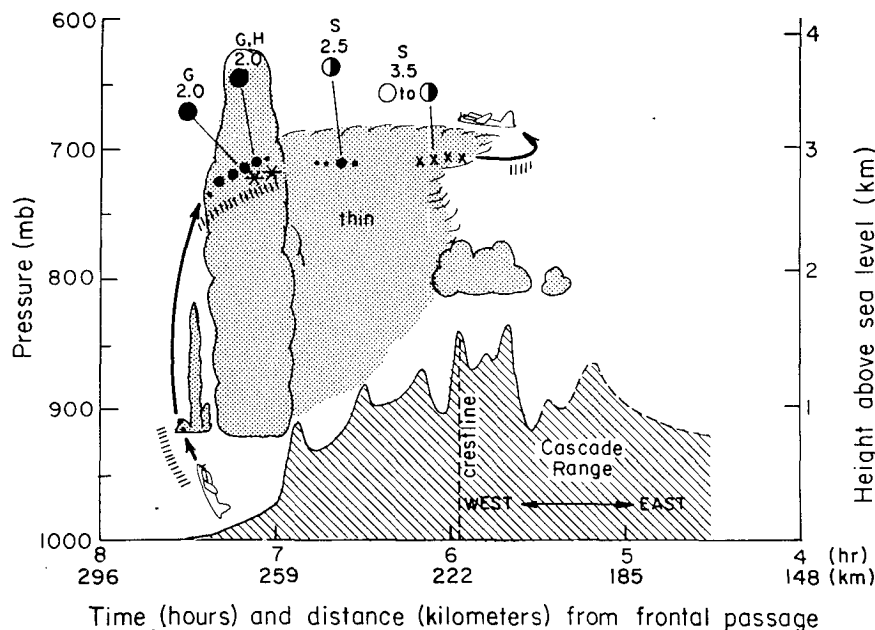


FIG. 13. Cloud configuration and microstructure over Cascade Range after frontal passage. For key to symbols see legend to Fig. 10.

are similar in format to Fig. 10, which showed the structure of the system as it was beginning to pass over the Cascade Range. In Figs. 11–13, however, the topography is emphasized by using height above sea level as the vertical coordinate rather than height above ground. It should be noted that the horizontal scale in Figs. 11–13 is not a geographical scale. The orographic features are positioned *relative to the front* according to the time the aircraft flew over them. The mountain profile appears stretched or contracted depending on whether the flight path was in the opposite or the same direction as the frontal motion.

The shape of the frontal surface in Figs. 11–13 is similar to that shown in Fig. 10, except that the boundary of the cold air mass has been displaced upward slightly to account for lifting of the air mass over the Cascade Range. The front could not be located more precisely since there were no rawinsonde data over the mountains.

From Figs. 11 and 12 it is noted that the large amount of cloud previously located ahead of the front (Fig. 10) was sharply reduced as the system crossed over the Cascade Range and the amount of cloud behind the front increased. The increase in cloudiness behind the front evidently occurred as orographic lifting on the western slope of the Cascade Range acted to offset post-frontal subsidence. The explanation for the decrease in the amount of cloud ahead of the front is not as obvious since the precipitation data discussed below in Section 8b indicate that *this decrease began on the windward (western) slope of the Range*. Therefore, it is not possible simply to invoke orographic sinking to

explain the decrease in the amount of cloud ahead of the front.

We suggest that the decrease in cloudiness ahead of the front was associated with blocking of low-level horizontal winds by the Cascade Range. From Section 6d it is recalled that moisture was fed into the frontal cloud almost entirely below the 800 mb level, the approximate average height of the Cascade Range. This moist flow was directed from the south-southwest (Fig. 6). With only a very weak westerly wind component, the low-level moist air ahead of the front was unable to flow over the Cascade Range, being blocked by the mountain barrier in the manner described by Fraser *et al.* (1973). The eastward progression of the approaching front, however, was not blocked by the Cascade Range and, as the front moved from the western foothills to the crest of the range, the low-level moisture west of the Cascade Crest was all lifted ahead of the front. With the low-level moisture source thus exhausted by the time the front had reached the Cascade Crest, the amount of prefrontal cloudiness had decreased markedly before the system was subjected to downslope orographic motion on the lee side of the Cascade Range.

Although much of the cloud mass seen ahead of the front in Fig. 10 had disappeared by the time of the flights shown in Figs. 11 and 12, the cloud microstructure observed in Figs. 12 and 13 suggests that frontal lifting was still playing a role in the formation of the clouds over the Cascade Range. The largest values of liquid water content, the largest concentrations of ice particles, and the most heavily rimed ice particles were

all found to the *lee of the Cascade Crest* and in the portion of the cloud mass which was *closest to the front*. If the clouds were entirely orographic in nature the most active portions would occur on the windward side of the crest. The cloud masses shown in Figs. 11 and 12 evidently were the result of a combination of frontal and orographic effects.

It is further noted that the relative positions of liquid water and ice shown in both Figs. 11 and 12 were similar to those in the purely frontal cloud of Fig. 10. In all three cases the leading (eastern) edge of the cloud mass is marked by a narrow zone of liquid water and very little or no ice. These properties characterize relatively young clouds. This zone was followed immediately to the west, in all three cases, by the region of highest ice particle concentration in the cloud. The remainder of the cloud in each case was composed of ice particles in reduced concentrations and only occasional liquid water. The similarity of internal cloud structure seen in Figs. 10, 11 and 12 suggests that frontal, rather than orographic, dynamics were dominant in the western portions of the cloud masses shown in Figs. 11 and 12.

Fig. 13 shows the cloud pattern encountered over the Cascade Range 6-8 h after the surface frontal passage. By this time the clouds were apparently purely orographic in origin. This orographic nature is evident by the fact that they were found almost exclusively on the windward slope of the range. In addition, the general cloud structure shown in Fig. 13 is quite unlike that observed earlier when the front was in the vicinity of the Cascade Range. In the earlier cases (Figs. 10-12) the *eastern* edge of the cloud system was consistently marked by a narrow zone of maximum liquid water content and low ice particle concentration followed immediately to the *west* by a zone of maximum ice concentration and low liquid water content. With the front no longer influencing the cloud formation processes (Fig. 13), the most active cloud was found over

the *western* (upwind) foothills of the mountain range where a narrow zone of liquid water and no ice was followed immediately to the *east* by a narrow zone of maximum ice concentration and reduced liquid water content. This reversal of microstructure implies that the cloud structure observed earlier over the Cascade Range (Figs. 12 and 13) was at least partially frontal in nature.

b. Precipitation

The change of the frontal cloud structure as the system progressed over the Cascade Range was investigated further by examining the hourly precipitation amounts from the network of National Weather Service raingage stations in Washington (NOAA, 1973). These data were composited under the assumption that the precipitation in central Washington was determined (i) by the proximity of the station to the Cascade Range (measured in distance ξ from the Cascade crestline) and (ii) by the position of the station in relation to the moving front (measured in time τ after the surface frontal passage). For a given hourly precipitation measurement, τ was measured from the midpoint of the observation hour.

The average hourly rainfall amounts for various positions relative to the front and to the mountains were calculated by averaging the hourly amounts for different combinations of τ and ξ and plotting the results in the coordinate system shown in Fig. 14. Grid boxes of size 1 h in $\Delta\tau$ and 18.5 km in $\Delta\xi$ were used in computing the averages. Contours of the average hourly precipitation amounts are shown in Fig. 15. As indicated in Fig. 14, various horizontal strips in this coordinate system may be identified with certain orographic regions, while vertical strips may be identified with frontal processes. The modification of the frontal precipitation by the Cascade Range will be discussed by comparing the rainfall patterns in the three or-

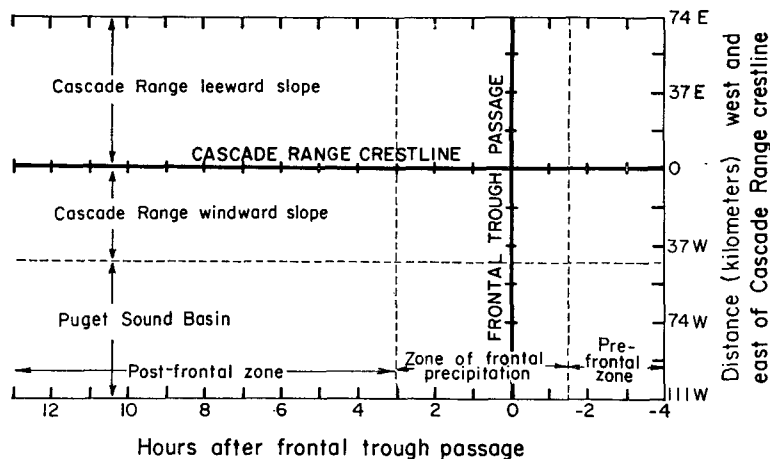


FIG. 14. Coordinate system used to separate frontal and orographic effects.

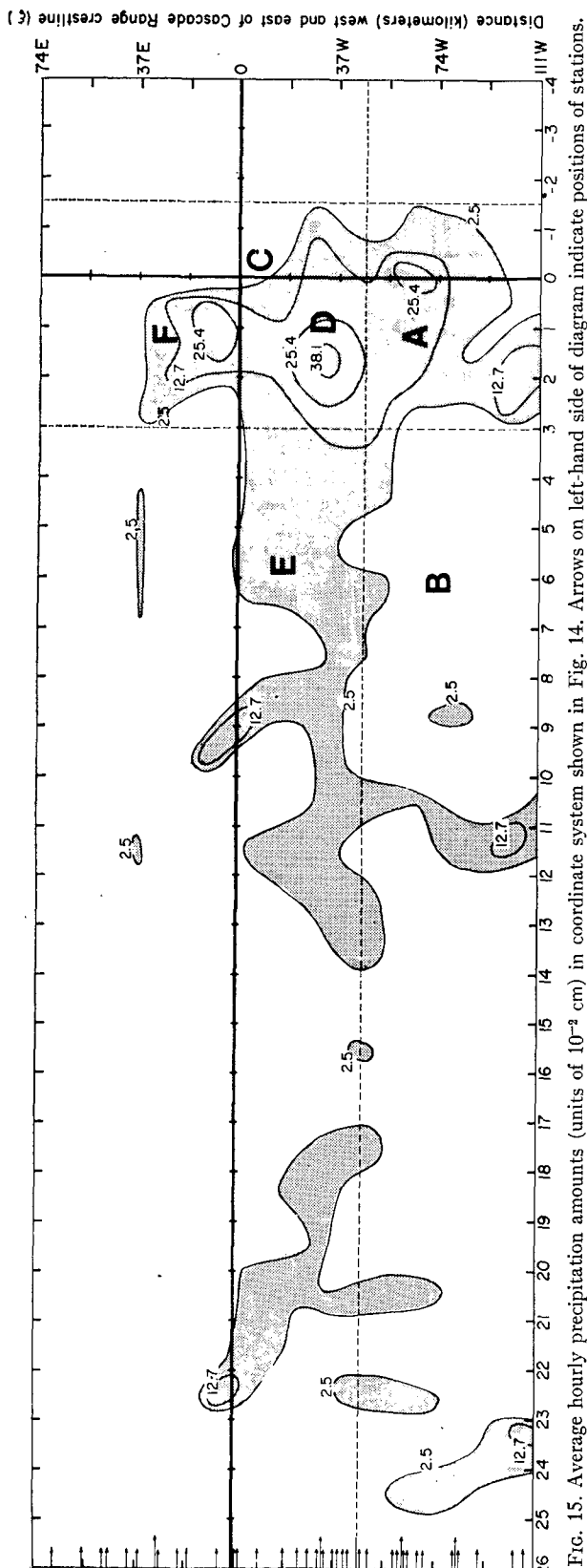


FIG. 15. Average hourly precipitation amounts (units of 10^{-3} cm) in coordinate system shown in Fig. 14. Arrows on left-hand side of diagram indicate positions of stations.

graphic (horizontal) strips of Fig. 15 (i.e. the Puget Sound Basin, the windward slope of the Cascade Range, and the leeward slope of the Cascade Range, as defined in Fig. 14).

The precipitation pattern in the Puget Sound Basin, as shown in Fig. 15, is in good agreement with the frontal structure assembled previously in Fig. 8b. The precipitation in the Puget Sound Basin was generally confined to the period extending from 1 h before the frontal passage to 3 h after the frontal passage (letter A in Fig. 15), and most of the precipitation fell immediately behind the surface front. The end of the precipitation 3 h after the frontal passage (see region B in Fig. 15) apparently was a result of the pronounced post-frontal subsidence which was noted previously in Figs. 8 and 9.

Several changes in the precipitation data were noted as the front moved over the windward slope of the Cascade Range (regions C, D and E in Fig. 15). It was mentioned above that much of the large cloud seen ahead of the front in Fig. 10 disappeared as the front moved across the range (recall Figs. 11 and 12). The precipitation data in region C of Fig. 15 show that leading edge of the frontal precipitation zone was also found increasingly later relative to the time of frontal passage as the system passed over the Cascade Range. In region C of Fig. 15 it is evident that this delay began on the *windward* slope of the Cascade Range.

In region D of Fig. 15, it is seen that just *behind the front* the frontal rainfall amounts were enhanced on the windward slope of the Cascade Range. Comparison of the average hourly precipitation amounts in regions A and D indicates that the frontal precipitation over the windward slope of the Cascade Range (D) exceeded that observed over the Puget Sound Basin (A) by a factor of 2 or 3. Orographic enhancement of the general level of cloudiness just behind the front as the system crossed the Cascade Range was noted previously in Figs. 11 and 12.

On the windward slope of the range, the frontal precipitation zone was followed by a long period of post-frontal precipitation (region E in Fig. 15). This period of precipitation contrasts sharply with the lack of a continuous period of post-frontal precipitation in the Puget Sound Basin (B in Fig. 15). Evidently, the orographic lifting on the windward slope of the range offset the post-frontal subsidence which had abruptly ended the rainfall 3 h after the frontal passage in the Basin area. The purely orographic, post-frontal clouds flown through by the aircraft and shown in Fig. 13 were typical of those producing the precipitation in region E of Fig. 15.

Although the post-frontal precipitation on the windward slope (E in Fig. 15) lasted for about 20 h, the amounts which fell were rather small and most of the precipitation occurred during the period of combined frontal and orographic precipitation (D in Fig. 15).

On the leeward side of the Cascade Range, the only significant precipitation occurred in the frontal zone itself (region F of Fig. 15). The cutting off of the front from its low-level moisture source west of the Cascades (see Section 8c) apparently continued to lead to an ever later onset of precipitation relative to the front. This effect combined with leeside subsidence lead to a complete disappearance of any frontal precipitation by the time the surface front was 37 km east of the Cascade Crest.

9. Conclusion

This study has documented the structure of a frontal cloud system on a wide range of scales. The results reaffirm those of several previous investigations in showing that mesoscale processes play an important role in the development of frontal precipitation. Among the more outstanding mesoscale features of the frontal system examined here are the following.

1) Alternating mesoscale tongues of low- θ_w and high- θ_w air were associated with the front. These tongues included a pre-frontal surge of low- θ_w air ahead of the occluded front, a low-level high- θ_w tongue along the occluded front, and mesoscale high- θ_w tongues in the cold air mass behind the occluded front. These tongues are similar to the tongues, or "hyperbaroclinic zones," found in occluded frontal systems by other investigators.

2) The cloud zone along the occluded front was dominated by a mesoscale circulation pattern similar to that of an organized convective system. The mesoscale circulation was 50 km wide and the updraft was fed by low-level high- θ_w air ahead of the front; the downdraft was fed by mid-level low- θ_w air behind the front. The vertical velocities in the updraft and downdraft zones were of the order of 10 cm s^{-1} on average. Thus the mesoscale circulation was not as vigorous as in other organized convective systems. A narrow, cumulus-scale core of more intense lifting was embedded within the larger-scale updraft zone at the leading edge of the frontal cloud.

The fact that features similar to those listed above have also been observed by other workers in widely varying geographical areas indicates that the occurrence of mesoscale structure in frontal systems is of global significance. It is now clear that the classical Norwegian frontal models present a highly idealized overview of frontal clouds and precipitation and that improvements in the forecasting of frontal precipitation can be expected only as the relationship between synoptic-scale dynamics and mesoscale structure become elucidated.

In the present study we have for the first time examined the cloud microphysics of a frontal system in the context of the observed synoptic and mesoscale structure. It appears from this preliminary study that the growth modes of precipitation particles in frontal clouds are also more complex than classical models

would suggest. According to Bergeron's (1935) ideas, the key factor in the growth of cloud particles to precipitation size would be the diffusional growth of ice crystals. However, our airborne observations show that the concentrations of ice particles in the frontal cloud were considerably in excess of those required for the efficient growth of precipitable particles from the vapor phase alone, and that growth by riming and aggregation played important roles.

This study has also provided an excellent opportunity to examine the modification of a frontal cloud system as it passes over a large mountain range. The amount of cloud ahead of the front decreased and amount of precipitation was delayed as the system passed over the Cascade Range, while the amount of cloud and precipitation behind the front increased. We attribute the decrease in cloudiness and delay in precipitation ahead of the front to the gradual cutting off of the frontal cloud from its source of moisture west of the Cascade Crest. The increase in cloud amount and precipitation behind the front was due to orographic lifting on the windward slopes.

Acknowledgments. Thanks are due to all members of the Cloud Physics Group who participated in the collection and interpretation of the data described in this paper. We are also grateful to Dr. Richard J. Reed for helpful discussions. This research was supported by the Atmospheric Sciences Section of the National Science Foundation under Grants GA-40806 and DES-7414726.

REFERENCES

- Austin, P. M., and R. A. Houze, Jr., 1972: Analysis of the structure of precipitation patterns in New England. *J. Appl. Meteor.*, **11**, 926-935.
- Bergeron, T., 1935: On the physics of cloud and precipitation. *Proc. Fifth Assembly UGGI*, Vol. 2, Lisbon, 156-178.
- , 1950: Ueber der mechanismen ausgiebigen Niederschlage. *Ber. Deut. Wetterd.*, **12**, 225-232.
- Bjerknes, J., 1919: On the structure of moving cyclones. *Geophys. Publ.*, **1**, No. 2, 8 pp.
- Braham, R. R., 1964: What is the role of ice in summer rain showers? *J. Atmos. Sci.*, **21**, 640-645.
- Browning, K., 1971: Radar measurements of air motion near fronts, Part 2: Some categories of frontal air motion. *Weather*, **26**, 320-340.
- , and T. W. Harrold, 1969: Air motion and precipitation growth in a wave depression. *Quart. J. Roy. Meteor. Soc.*, **95**, 288-309.
- , and —, 1970: Air motion and precipitation growth at a cold front. *Quart. J. Roy. Meteor. Soc.*, **96**, 369-389.
- , and C. W. Pardoe, 1973: Structure of low-level jet streams ahead of mid-latitude cold fronts. *Quart. J. Roy. Meteor. Soc.*, **99**, 619-638.
- Elliott, R. D., and E. L. Hovind, 1964: On convection bands within Pacific coast storms and their relation to storm structure. *J. Appl. Meteor.*, **3**, 143-154.
- , and —, 1965: Heat, water, and vorticity balance in frontal zones. *J. Appl. Meteor.*, **4**, 196-211.
- Fletcher, N. H., 1962: *The Physics of Rainclouds*. Cambridge University Press, 390 pp.
- Fraser, A. B., R. C. Easter and P. V. Hobbs, 1973: A theoretical study of the flow of air and fallout of solid precipitation over

- mountainous terrain: Part I: Airflow model. *J. Atmos. Sci.*, **30**, 801-812.
- Harrold, T. W., 1973: Mechanisms influencing the distribution of precipitation within baroclinic disturbances. *Quart. J. Roy. Meteor. Soc.*, **99**, 232-251.
- Hobbs, P. V., 1969: Ice multiplication in clouds. *J. Atmos. Sci.*, **26**, 315-318.
- , 1973: Anomalously high ice particle concentrations in clouds. Invited review paper. *Proc. Eighth Intern. Con. on Nucleation*, Leningrad (in press).
- , and D. G. Atkinson, 1975: The concentrations of ice particles in orographic clouds and cyclonic storms over the Cascade Mountains. Submitted to *Quart. J. Roy. Meteor. Soc.*
- , L. F. Radke, A. B. Fraser, J. D. Locatelli, C. E. Robertson, D. G. Atkinson, R. J. Farber, R. R. Weiss and R. C. Easter, 1971: Studies of winter cyclonic storms over the Cascade Mountains (1970-71). Contributions from the Cloud Physics Group, Res. Rept. 6, University of Washington.
- , —, J. D. Locatelli, D. G. Atkinson, C. E. Robertson, R. R. Weiss, F. M. Turner and R. R. Brown, 1972: Field observations and theoretical studies of clouds and precipitation over the Cascade Mountains and their modification by artificial seeding (1971-72). Contributions from the Cloud Physics Group, Res. Rept. 7, University of Washington.
- Houghton, H. G., 1968: On precipitation mechanisms and their artificial modification. *J. Appl. Meteor.*, **7**, 851-859.
- Kreitzberg, C. W., 1964: The structure of occlusions as determined from serial ascents and vertically-directed radar. Res. Rept. AFCRL-64-26, Air Force Cambridge Research Laboratories, L. G. Hanscom Field, Mass., 121 pp.
- , and H. A. Brown, 1970: Mesoscale weather systems within an occlusion. *J. Appl. Meteor.*, **9**, 417-432.
- Locatelli, J. D., and P. V. Hobbs, 1974: Fall speeds and masses of solid precipitation particles. *J. Geophys. Res.*, **79**, 2185-2197.
- Magono C., and C. W. Lee, 1966: Meteorological classification of natural snow crystals. *J. Fac. Sci., Hokkaido Univ.*, Ser. VII, **2**, No. 4.
- Mossop, S. C., 1970: Concentrations of ice crystals in clouds. *Bull. Amer. Meteor. Soc.*, **51**, 474-478.
- , A. Ono and K. J. Heffernan, 1967: Studies of ice crystals in natural clouds. *J. Rech. Atmos.*, **3**, 45-64.
- Newton, C. W., 1963: Dynamics of severe convective storms. *Meteor. Monogr.*, **5**, No. 27, 33-58.
- NOAA, 1973: Hourly Precipitation Data—Washington. Vol. 23, No. 3, Environmental Data Service.
- Saucier, W. J., 1955: *Principles of Meteorological Analysis*. The University of Chicago Press, 438 pp.
- Turner, F. M., and L. F. Radke, 1973: The design and evaluation of an airborne optical ice particle counter. *J. Appl. Meteor.*, **12**, 1309-1318.
- Zipser, E. J., 1969: The role of organized unsaturated convective downdrafts in the structure and rapid decay of an equatorial disturbance. *J. Appl. Meteor.*, **8**, 799-814.